Reac Kinet Mech Cat (2017) 122:69–83
DOI 10.1007/s11144-017-1223-x

Glycerol steam reforming over calcium deficient hydroxyapatite supported nickel catalysts

Marcin Cichy[1] · **Justyna Dobosz**[2] · **Tadeusz Borowiecki**[1] · **Mirosław Zawadzki**[2]

Received: 10 April 2017 / Accepted: 12 July 2017 / Published online: 21 July 2017

Abstract This paper presents reports on the glycerol steam reforming reaction. The studies were performed over four nickel catalysts with different metal loading (up to 10 wt%) supported on calcium deficient hydroxyapatite (DHAp). The support was synthetized by the microwave assisted hydrothermal method. The steam reforming reaction was performed under atmospheric pressure in the 650–800 °C temperature range using 10 mg of catalyst sample and a glycerol/water mixture with S/C = 3. All catalysts were well characterized by physicochemical methods (XRD, XRF, TPR, HRTEM). The catalytic tests results were presented by means of glycerol conversion, hydrogen and carbon containing gases selectivity. The most promising results were obtained for catalyst with moderate Ni content (~7.5 wt%), which proved to be stable during a few hours on-stream and provided glycerol conversion at least 94% at reaction temperature above 750 °C.

Keywords Glycerol · Steam reforming · Syngas · Hydroxyapatite

Introduction

The high growth of fossil fuels prices and tightening environmental requirements, which restrict emissions of the contaminants released to the atmosphere affected the increase of the share of energy possessed from renewable sources, including

✉ Marcin Cichy
marcin.cichy@umcs.pl

[1] Department of Chemical Technology, Faculty of Chemistry, Maria Curie-Skłodowska University, Lublin, Poland

[2] W. Trzebiatowski Institute of Low Temperature and Structure Research, Polish Academy of Sciences, Wrocław, Poland

biomass. One of the most popular ways of processing vegetable oils is their transesterification, which leads to obtaining so-called biodiesel. This process gives, beside the main product, technological waste, which is glycerol fraction. This waste contains up to 80% of glycerol and constitute average $\sim$10 wt% of produced esters. In the European Union, biodiesel use is projected to increase from 12.7 billion L in 2014 to its highest level of almost 14.8 billion L in 2020 and world biodiesel production is expected to grow up to $\sim$38 billion L in 2024 [1]. This means a significant increase of biodiesel production concluding in rising problems related to the utilization of the glycerol waste fraction.

Beside the already known applications of glycerol in pharmaceutical, food, cosmetics and tobacco industry or explosive materials, scientists began to propose new processes having their purposes in fitting up this waste (e.g. receiving such chemicals as dihydroxyacetone [2, 3], 1,3-propanediol [4–6], glycerol ethers [7, 8] and glycerol esters [9, 10]). As a result of dehydration, acrolein can be obtained, which is an important chemical compound used for the production of acrylic acid [11]. Glycerol can be used as a biocomponent to engine fuels and even can be burned as a fuel. Wide information about classical and novel glycerol phase utilization processes can be found in reviews [12–14].

Another way of the utilization of high amounts of glycerol waste fraction could be a process of its conversion to the hydrogen and synthesis gases, on which products is still growing demand (e.g. for hydrogen fuel cells) [15]. The literature data show few routes in which this process could be realized: aqueous phase reforming [16], autothermal reforming [17], gasification in supercritical water [18] and steam reforming [19–24]. Especially big hopes are connected with the steam reforming reaction.

Glycerol can be converted into syngas by the steam reforming process according to the following reaction:

$$C_3H_8O_3 + 3H_2O \rightarrow 3CO_2 + 7H_2 \quad (1)$$

This overall reaction can be written as two separate processes: glycerol decomposition to hydrogen and carbon monoxide (2) and followed by the water–gas shift reaction (3):

$$C_3H_8O_3 \rightarrow 3CO + 4H_2 \quad (2)$$

$$CO + H_2O \leftrightarrow CO_2 + H_2 \quad (3)$$

From many catalytic systems used for glycerol steam reforming, those based on metals such as Ru [18, 25, 26], Rh [17, 26], Ir [26–28], Pd [26, 29, 30], Pt [17, 26, 31–34], and Co [27] can be mentioned. Different supports were also used including CeO_2 [25, 27, 35, 36], Al_2O_3 [24–26, 37], MgO [35], TiO_2 [35] and ZrO_2 [36]. However, the most investigated catalysts are those based on nickel [26, 27, 30, 33, 35, 38–43].

Apatites are a group of compounds with the general formula $M(1)_4M(2)_6(BO_4)_6(X)_2$, where M(1) and M(2) are a divalent metal cations (mainly Ca^{2+}, Sr^{2+}, Ba^{2+}, Cd^{2+} or Pb^{2+}), B is metalloid (primarily P^{5+}) and X is a monovalent anion (OH^-,

Cl^-, F^- or Br^-) [44, 45]. These compounds commonly crystallize in hexagonal ($P6_3/m$) phase [44]. Among this large class of minerals, calcium phosphate hydroxyapatite (HAp, $Ca_{10}(PO_4)_6(OH)_2$) is the most well-known apatite compound. HAp is an inorganic component of vertebrate bones and due to its high biocompatibility with bone tissue has been widely studied for application in medicine, especially in the implantation medicine [46]. Nevertheless, HAp is also an interesting catalytic material. It is characterized by very good thermal stability over a wide range of temperatures as well as resistance to deactivation processes, so by features which are desired from the point of view of application in the catalysis [47, 48]. The hydroxyapatite shows a mesoporous structure, well-developed surface area and high porosity [49]. Therefore, it can be used as catalyst support. It is worth mentioning that the acid–base properties of HAp can be easily changed by modifying Ca/P ratio. The surface acidity of HAp increases with a decrease in the Ca/P ratio [50]. Calcium-deficient (non-stoichiometric) HAp is given by the formula $Ca_{10-x}(HPO_4)_x(PO_4)_{6-x}(OH)_{2-x}$ (x is the number of cationic vacancies) [47]. The catalytic activity of calcium hydroxyapatite has been reported, for example, in the removal of oxygenated volatile organic compounds [47] or the oxidative coupling of methane [51].

There are a few reports in the literature concerning the use of hydroxyapatite in processes of hydrogen production. Ashok et al. [52] have used HAp as a support of nickel catalysts in the decomposition reaction of methane ($CH_4 \rightarrow C + 2H_2$). It was found that the "pure" hydroxyapatite (without nickel ions) is not active in this process. The catalytic activity of $Ca_{10}(PO_4)_6(OH)_2$ increased after the incorporation of the nickel ions, which allowed to obtain a maximum value of the hydrogen yield at level 550 mmol H_2/g_{cat}. The glycerol steam reforming process over catalysts supported on hydroxyapatites was studied only by Wan Daud et al. The research was focused on nickel catalysts [53–55] and nickel-cerium-copper catalysts [49] supported on commercial HAp (Sigma-Aldrich). Tests conducted on nickel catalysts (ion concentrations: 3, 6 and 12 wt%) showed that the most efficient catalytic system for the steam reforming of glycerol was 3 wt% Ni/HAp. The high catalytic activity of this system was assigned to its high surface area.

The aim of this work was the evaluation of non-stoichiometric hydroxyapatite based nickel catalysts during the glycerol steam reforming reaction.

Experimental

Catalyst synthesis

It is well known that products formed during glycerol steam reforming depend on the acid–base properties of tested material. The presence of a large number of acid sites induces the secondary reaction that leads to liquid formation and coke formation [56]. On the other hand, the large number of base sites favors glycerol transformation to such products as 1,2-propanediol or acetone [57]. So, it is important to obtain the hydroxyapatite with such distribution of acid and base sites

which ensure the highest hydrogen yield and the lowest amount of undesirable products.

Calcium deficient hydroxyapatite ($Ca_9(HPO_4)(PO_4)_5(OH)$, DHAp) was synthesized under hydrothermal conditions. Calcium nitrate ($Ca(NO_3)_2{\cdot}6H_2O$, POCH) and diammonium phosphate ($(NH_4)_2HPO_4$, POCH) were dissolved in 25 and 10 mL of distilled water, respectively. Then, $(NH_4)_2HPO_4$ solution was added into $Ca(NO_3)_2{\cdot}6H_2O$ solution under vigorous stirring. The pH was adjusted to about 10 by 25% ammonia water (NH_4OH, POCH) addition. Next, the precipitation was decanted into a Teflon vessel and placed in a microwave reactor (ERTEC, MAGNUM II) under the pressure of 50 bar at 200 °C for 1 h. After hydrothermal treatment, the product was filtered, washed with distilled water and 96% ethanol (POCH) several times and dried at 80 °C for 24 h. Finally, the white powder was calcined at 500 °C for 3 h under atmospheric conditions. As a result, DHAp was obtained.

DHAp supported nickel catalysts were prepared by the incipient wetness impregnation. An aqueous nickel nitrate solution ($Ni(NO_3)_2{\cdot}6H_2O$, POCH) was used as precursor of nickel species. After the impregnation process, the samples were dried at 30 °C for 24 h and then calcined at 500 °C for 3 h. The catalysts containing four different nickel amounts were denoted as Ni(2.5)/DHAp, Ni(5.0)/DHAp, Ni(7.5)/DHAp and Ni(10.0)/DHAp.

Catalysts characterization

The nickel content in the catalyst was determined by energy dispersive X-ray fluorescence (ED-XRF) analysis using a Canberra Packard fluorescence spectrometer equipped with a liquid N_2-cooled Si(Li) detector. The AXIL software package for spectra deconvolution and for calculation of Ni content was used.

The Brunauer–Emmett–Teller (BET) surface area of the catalysts was determined by low-temperature (−196 °C) nitrogen adsorption in the ASAP 2405 N v1.0 apparatus (Micromeritics). The pore volume and their average diameter were evaluated applying the Barrett–Joyner–Halenda (BJH) method.

The active metal surface area, dispersion of the nickel phase and mean size of the nickel particle in catalysts were calculated from the hydrogen chemisorption data obtained in the AUTOSORB-1CMS apparatus (Quantachrome Instruments) at 30 °C. The amount of surface metal atoms was calculated from that of hydrogen chemisorbed, assuming that one hydrogen atom is adsorbed on the area occupied by one surface nickel atom (the stoichiometry of chemisorption is Ni/H = 1/1) and that the surface area occupied by one atom of hydrogen is equal to 0.065 nm^2 [58]. The total H_2 uptake was determined by extrapolation of the linear part of the isotherm to the zero pressure. The following equation was used to calculate active surface area:

$$S_{H_2} = \frac{V_{H_2} \cdot N \cdot A_{H_2}}{22414} [m^2/g] \quad (4)$$

Here V_{H_2} is the hydrogen volume chemisorbed at saturated monolayer (cm^3), N is the Avogadro constant, A_{H_2} is the surface occupied by hydrogen molecule ($Å^2$).

Temperature-programmed reduction (TPR) experiments were carried out with an Autochem II 2920 apparatus (Micromeritics) equipped with a thermal conductivity detector (TCD) and LN_2 water trap. The reduction profile was obtained by passing 5% H_2/Ar flow at the rate of 30 mL min^{-1} through 0.05 g of the catalyst (0.3–0.6 mm). The temperature was increased from 30 to 800 °C at the rate of 10 °C min^{-1}.

The X-ray powder diffraction (XRD) patterns in Bragg–Brentano geometry were recorded on a Empyrean X-ray (PANalytical) diffractometer equipped with a PIXcel^{3D} detector and operated at 40 kV and 25 mA using Cu K_α radiation ($\lambda = 0.154$ nm). Data were acquired from 10 to 110° (2θ) with a 0.026° (2θ) step size. The measured patterns were compared with the HighScore Plus database for phase identification. The crystallite size was calculated using the Scherrer equation. The correction for instrumental broadening was applied with the reference standard (LaB_6).

HRTEM images were obtained using a Titan G2 60-300 (FEI) electron microscope equipped with field emission gun, monochromator, a system of three condenser lenses, a C_s image corrector, a high angle annular dark field detector (HAADF) and energy dispersive X-ray spectrometer (EDS). The microscopic examination of the catalysts was carried out at an accelerating voltage of the electron beam of 300 kV.

Catalytic performance tests

The steam reforming of glycerol over Ni/DHAp catalysts was conducted in a continuous down-flown fixed-bed quartz tubular reactor under atmospheric pressure within temperature range of 650–800 °C (in 50 °C steps). 10 mg of catalyst sample (0.3 − 0.6 mm), between two quartz wool layers, was loaded into reactor. Before each measurement, the catalysts was reduced by heating up to 800 °C in hydrogen stream (20 mL/min) and then hold in this conditions for 2 h. The aqueous solution of glycerol with S:C = 1:3 was introduced to the reactor by syringe pump with feed flow rate (FFR) 0.066 mL/min. Helium was used as the carrier gas (10 mL/min). Before the mixture reached the catalyst bed, it passed a vaporizer where it was heated above 290 °C. The outlet products were condensed and separated into gas and liquid fractions. Gases were analyzed chromatographically (H_2, CO, CO_2, CH_4 and C_2H_4) by GC-8340 (Fisons) equipped with a TCD detector and HayeSep DB (Alltech) packed column. Analysis takes place every 12 min (5 measurements per reaction temperature). The liquid phase was determined for unreacted glycerol every 30 min (2 measurements per reaction temperature) by GC-2010 (Shimadzu) with FID detector using ZB-Wax Plus (Phenomenex) capillary column. The performance of the catalysts is presented in terms of H_2 selectivity, glycerol conversion degree as well as CO, CO_2, CH_4 and C_2H_4 selectivity, calculated from the following Eqs. 5–7:

$$\text{Glycerol conversion } (\%) = \frac{\text{Glycerol in} - \text{Glycerol out}}{\text{Glycerol in}} \times 100 \qquad (5)$$

$$H_2 \text{ selectivity } (\%) = \frac{H_2 \text{ moles produced}}{\text{C atoms in gas product}} \times \frac{1}{RR} \times 100 \quad (6)$$

$$\text{Selectivity of i } (\%) = \frac{\text{C atoms in species i}}{\text{C atoms in gas product}} \times 100 \quad (7)$$

Here RR is the reforming ratio (7/3), defined as the ratio of moles of H_2 to CO_2 formed, and species i is either one of CO, CO_2, CH_4 and C_2H_4.

For the selectivity (to hydrogen and carbon containing gases) results, the standard deviation was calculated.

Also, during liquid product analysis, oxygenates other than glycerol were noticed. There were trace amounts of these compounds and they were not taken into account in the calculations i.e. [59, 60].

Results and discussion

Catalysts characterization

The physicochemical properties of the DHAp support and calcined Ni/DHAp catalysts are summarized in Table 1. Table 2 presents results obtained for catalysts reduced at 800 °C in a hydrogen stream for 2 h. The introduction of nickel to the hydroxyapatite support and catalyst calcination do not cause significant changes in the characteristics of the samples. An increase in the amount of nickel resulted in a systematic, though small changes in BET surface area, as well as pore volume and average pore diameter. Also with increasing amounts of nickel, major changes in the complex, but very similar porous structure of calcined catalysts were observed (Fig. 1a).

The deficient nature of hydroxyapatite was confirmed by EDS measurements. The results show the Ca/P ratio of 1.57, which is less than for stoichiometric HAp (Ca/P = 1.67).

The reduction of the catalysts at 800 °C resulted in more than triple reduction of the total area and a significant decrease of the pore volume (Table 2). A surprising effect of the amount of nickel on the pore volume was found. The smallest pore volume showed catalysts with moderate (5–7.5 wt%) nickel content. It is noteworthy that all the samples of the calcined catalyst have very similar porous

Table 1 Physicochemical properties of DHAp support and calcined catalysts

Support/catalyst	S_{BET} (m^2/g)	V_p (cm^3/g)	D_p (nm)
DHAp	45	0.43	35
Ni(2.5)/DHAp	43	0.40	33
Ni(5.0)/DHAp	42	0.39	33
Ni(7.5)/DHAp	41	0.36	31
Ni(10.0)/DHAp	39	0.30	26

Table 2 Physicochemical properties of catalysts reduced at 800 °C

Catalyst	Ni content (wt%)	S_{BET} (m^2/g)	V_p (cm^3/g)	D_p (nm)
Ni(2.5)/DHAp	2.6	13	0.12	37
Ni(5.0)/DHAp	5.3	12	0.05	24
Ni(7.5)/DHAp	7.9	12	0.05	25
Ni(10.0)/DHAp	9.9	12	0.10	41

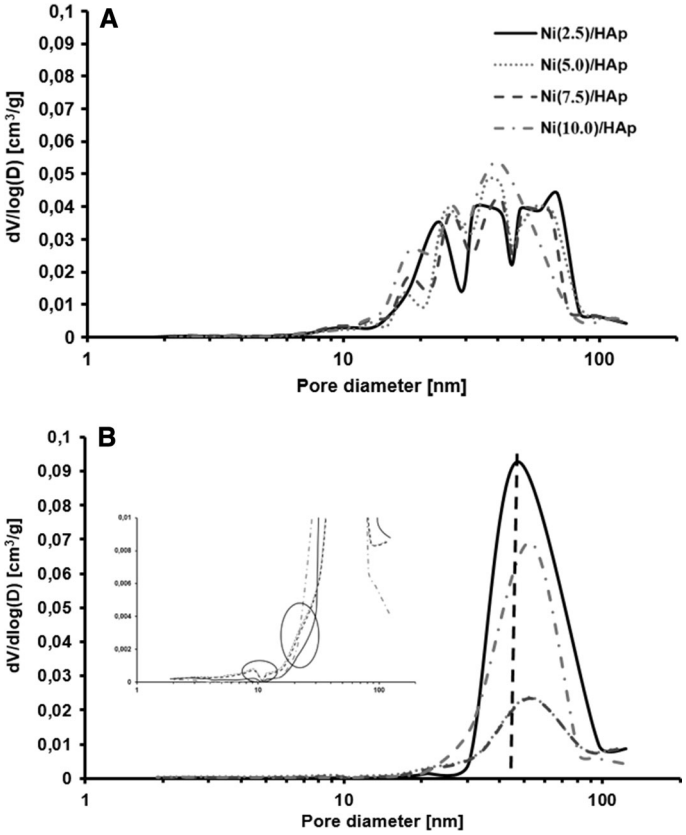

Fig. 1 Pore size distribution curves of "fresh" (**a**) and reduced in H_2 at 800 °C (**b**) Ni/DHAp catalysts

structure. The pore volume changes have no connection with increasing amounts of nickel.

The reduction process fundamentally changed the porous structure of catalysts causing the loss of a few distinguished groups of pores of different diameter. The

pore distribution curve shows a single peak, and the change of nickel amount in the catalysts does not influence its location (45–50 nm) (Fig. 1b).

The inset in Fig. 1b shows that a small amount of pores with diameters below 10 nm were also present. This applies only to catalysts with moderate Ni concentration (5–7.5 wt%).

The observed changes in the textural properties are connected with the reduction temperature. Under such conditions, the hydroxyapatite support undergoes sintering phenomena. A similar effect was observed in works [61, 62] and is related with changes in the shape of DHAp particles.

Fig. 2 presents the TPR profiles of hydroxyapatite and Ni/DHAp catalysts. As can be seen, in the tested temperature range, the DHAp support did not undergo any changes. For the nickel catalysts obtained results indicate the relatively complex structure of the reduction, especially at higher nickel contents. Changes in the TPR curves suggest that as the amount of nickel catalysts increases the share of difficult reducible NiO is higher. This NiO form, practically absent in the Ni(2.5)/DHAp catalyst, becomes dominant in catalysts containing 7.5 and 10 wt% of nickel. The first maximum can be assigned to the reduction of small particles of Ni, which have strong interaction with the support. The following peak located at higher temperatures may be related to the reduction of Ni^{2+} ions incorporated in the Ca(I) and Ca(II) sites of DHAp. Similar results were obtained by Jun et al. [63]. Also, with increasing amounts of nickel in the catalysts, a slight facilitation of NiO reduction was observed with the maximum at 350 °C. Literature data show different information about the influence of the amount of nickel on the course of the reduction step in Ni(x)/CaHAp catalysts, where (x) changed from 1 up to 10 wt% [53]. Increasing the nickel content resulted in a significant increase in the amount of more easily reducing form of NiO. The second difference between the described results is the high temperature at which the reduction takes place. For the catalysts of major contents of nickel (8 and 10%), reduction begins at a temperature of

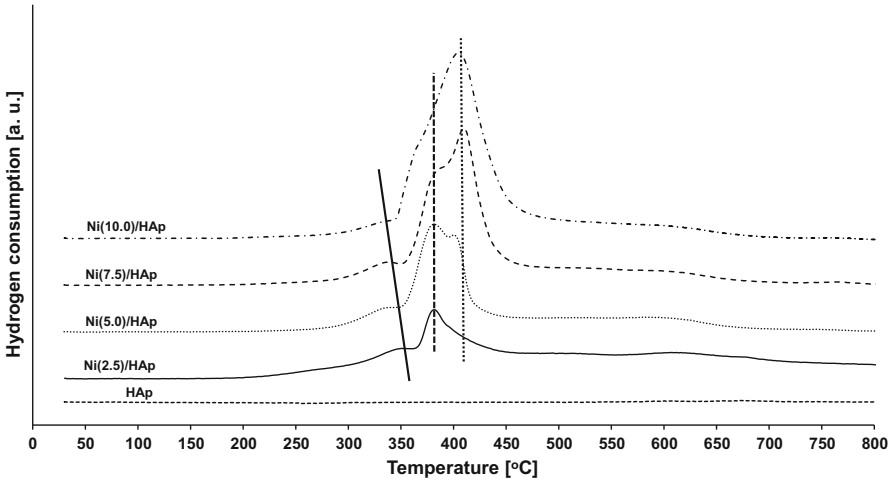

Fig. 2 TPR profiles of DHAp and Ni/DHAp catalysts

approximately 300 °C, but extends up to temperatures of 700 and 750 °C, having several peaks at temperatures around 410, 505, 620 and 720 °C [64]. The temperature-programmed reduction of a nickel catalyst (13.5 wt%) supported on commercial hydroxyapatite (Sigma-Aldrich) runs in a much wider temperature range [51]. Although the shape of the curve of the reduction is very similar to the TPR curve of Ni(10.0)/DHAp (Fig. 2), the reduction takes place at higher temperatures, 800 °C. The differences between the described catalysts are related to the methods of their preparation. In the case of the investigated catalysts, the support was prepared by a hydrothermal method under increased pressure assisted by microwave with subsequent impregnation. In [64], the method of coprecipitation of hydroxyapatite and its impregnation was used, and in [65], catalysts were obtained by the impregnation of ready support.

The XRD diffraction patterns of the reduced at 800 °C Ni/DHAp catalysts are shown in Fig. 3. X-ray analysis showed presence of several crystallographic phases: regular nickel (ICDD: 01-071-4654), hexagonal hydroxyapatite $Ca_5(PO_4)_3OH$ (ICDD: 00-024-0033) and monoclinic calcium phosphate $Ca_3(PO_4)_3$ (ICDD: 00-029-0359). The only observed difference between obtained patterns is intensity of the Ni (111) at the angle $2\theta = 44.4°$. The positions of diffraction peak maxima referred to hydroxyapatite ($2\theta = 31.74°$ and 32.86°) are consistent with literature data [54].

Table 3 summarizes data regarding the catalysts' active surface area, nickel dispersion and average Ni crystallites size. In fact, the Ni(2.5)/DHAp catalyst contained low metal concentration ($\sim$2.5 wt%), and it was impossible to determine its crystallites size by XRD method (d_x). The Ni/DHAp catalysts are characterized by relatively inactive surface area, which increases with an increasing amount of nickel. The increase in the absolute size of the active surface is accompanied by a decrease in the dispersion of nickel determined from the measurements of hydrogen

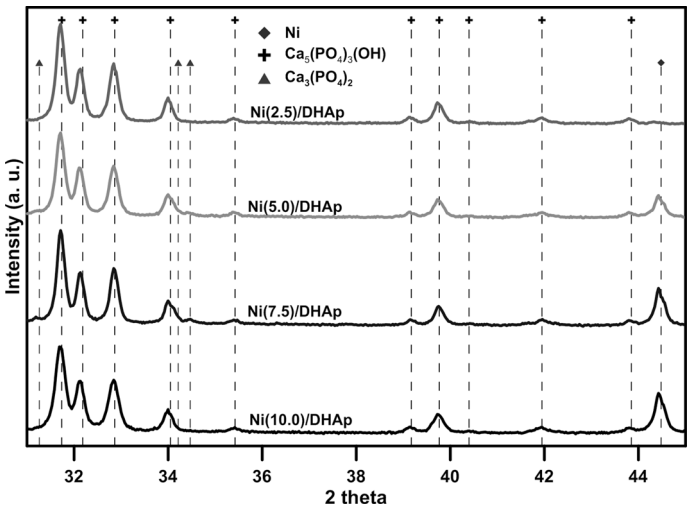

Fig. 3 Diffraction patterns of the reduced in H_2 at 800 °C Ni/DHAp catalysts in 31–45° angle range

Table 3 Results obtained from the hydrogen chemisorption and XRD studies

Catalyst	S_{H_2} (m^2/g)	Ni dispersion (%)	Mean size of Ni crystallites (nm)	
			d_H	d_X
Ni(2.5)/DHAp	0.66	3.9	27	–
Ni(5.0)/DHAp	0.72	2.1	49	64
Ni(7.5)/DHAp	0.77	1.5	69	67
Ni(10.0)/DHAp	0.93	1.4	71	57

chemisorption (d_H). Such changes to the average nickel crystallite size were not confirmed by the results obtained by X-ray diffraction studies (Table 3). Low Ni dispersion in reduced catalysts is strictly connected with textural changes of the support, which took place during reduction step. The metal dispersion also influences the sintering of nickel particles, which can occur during reduction: while the metal content increases, nickel dispersion decreases.

Fig. 4 presents images of calcined (A) and reduced (B) Ni(7.5)/DHAp catalyst, obtained by high resolution transmission electron microscopy (HRTEM). Samples calcined at 500 °C showed the elongated shape of the hydroxyapatite support having an average length of ~75 nm and an average width of ~35 nm. In the TEM images, it was difficult to observe particles derived from NiO, whose presence is confirmed by measurements of powder diffraction analysis. However, the absence of NiO particles in TEM images has not been explained yet and further research will be conducted. The reduction process at 800 °C causes changes in the support crystallite morphology, which can be connected with the sintering of hydroxyapatite particles.

Fig. 5 presents HRTEM images of reduced at 800 °C Ni(2.5)/DHAp (a) and Ni(7.5)/DHAp (b) catalysts. In both pictures, the nickel active sites are highly

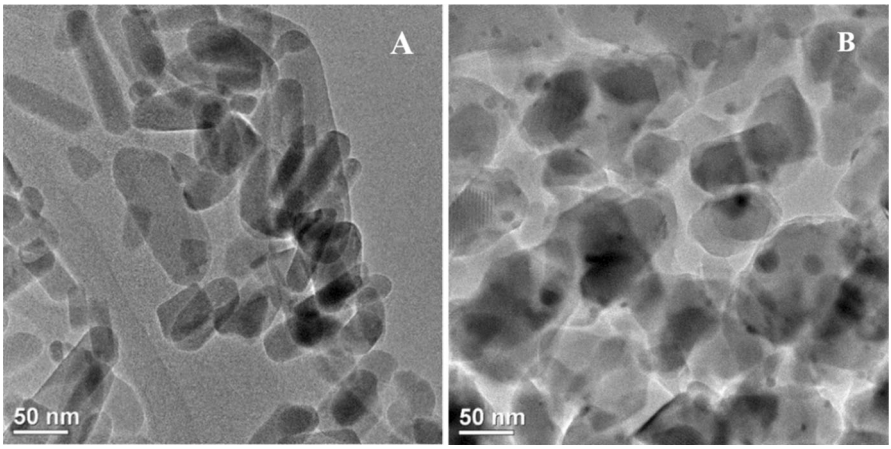

Fig. 4 TEM images of Ni(7.5)/DHAp catalyst: calcined (**a**) and reduced in H_2 at 800 °C (**b**)

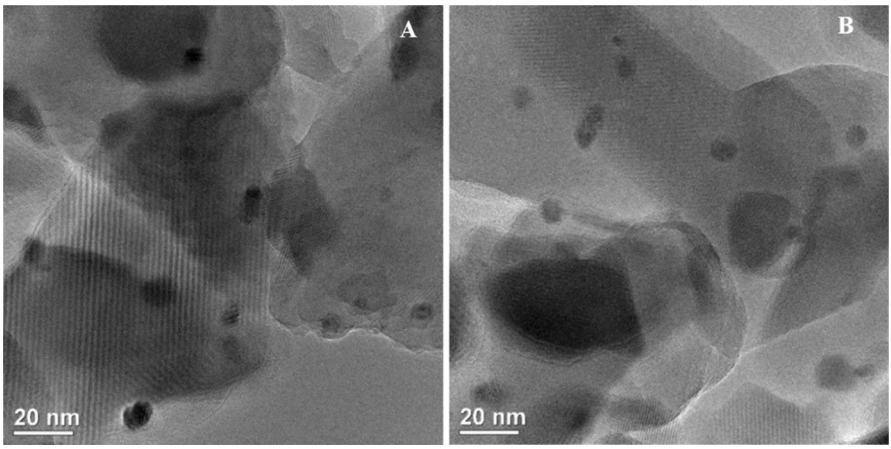

Fig. 5 TEM images of reduced in H_2 at 800 °C Ni(2.5)/DHAp (**a**) and Ni(7.5)/DHAp (**b**) catalysts

visible. On the DHAp support surface, small Ni crystallites, ranging in size from few to several tens of nm, are present.

Fig. 6 presents HRTEM images of nickel particles on the DHAp surface of Ni(2.5)/DHAp (a) and Ni(7.5)/DHAp (b) catalysts reduced at 800 °C at high magnification. Highly visible is the difference between Ni crystallites in both catalysts.

Catalytic performance tests

Catalyst activity in the glycerol steam reforming reaction presented as the glycerol conversion rate (X_{Gl}) shows Fig. 7. It strictly depends on the reaction temperature

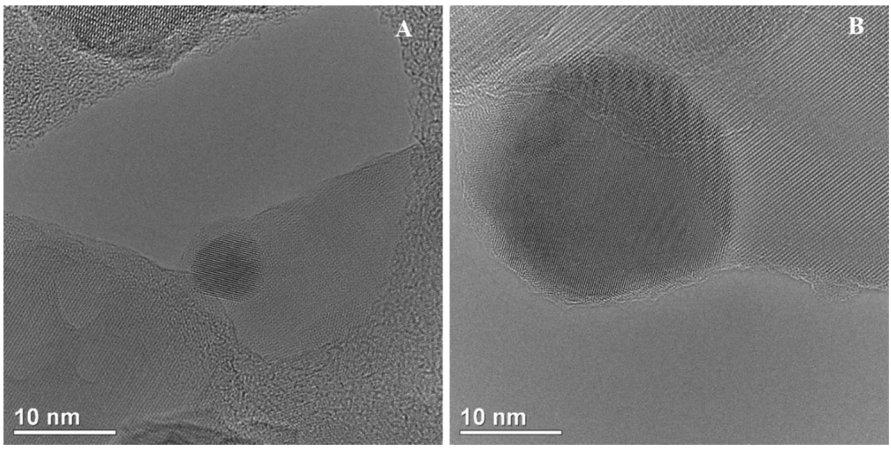

Fig. 6 TEM images of Ni crystallites sites in reduced in H_2 at 800 °C Ni(2.5)/DHAp (**a**) and Ni(7.5)/DHAp (**b**) catalysts

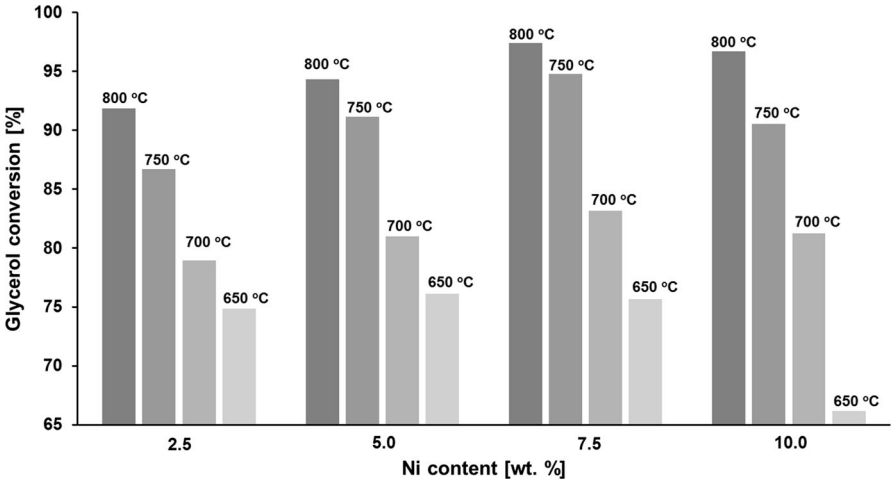

Fig. 7 Glycerol conversion over Ni/DHAp catalysts. Experimental conditions: 10 mg catalyst sample reduced in H_2 at 800 °C, S/C = 3, atmospheric pressure, 650–800 °C temperature range

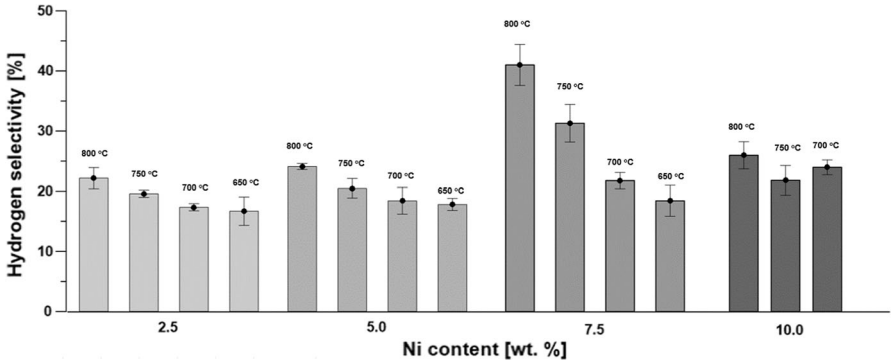

Fig. 8 Ni/DHAp catalysts hydrogen selectivity. Experimental conditions: 10 mg catalyst sample reduced in H_2 at 800 °C, S/C = 3, atmospheric pressure, 650–800 °C temperature range

and decreases with a temperature drop for all tested catalysts. The increase of the nickel content up to approximately 8 wt% increased the conversion of glycerol. Further increasing the amount of nickel resulted in decreases in the conversion temperatures $\leq$750 °C. The highest values of X_{Gl} were obtained at 800 °C for Ni(7.5)/DHAp catalyst ($\sim$98%). An increase of nickel concentration in the catalysts causes changes in hydrogen selectivity (S_{H_2})(Fig. 8). The catalysts containing 2.66 and 5.3 wt% of Ni showed similar, but very low S_{H_2}) values (<25%). Definitely, the best results showed Ni(7.5)/DHAp catalyst, for which, however, the selectivity was only 40% at 800 °C. Further increases of nickel content decreased the hydrogen selectivity.

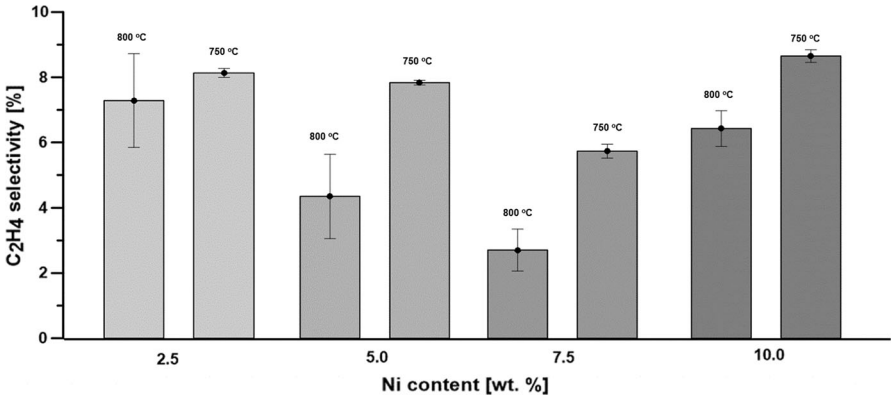

Fig. 9 Effect of the Ni loading in Ni/DHAp catalysts on ethylene selectivity. Experimental conditions: 10 mg catalyst sample reduced in H_2 at 800 °C, S/C = 3, atmospheric pressure, 650–800 °C temperature range

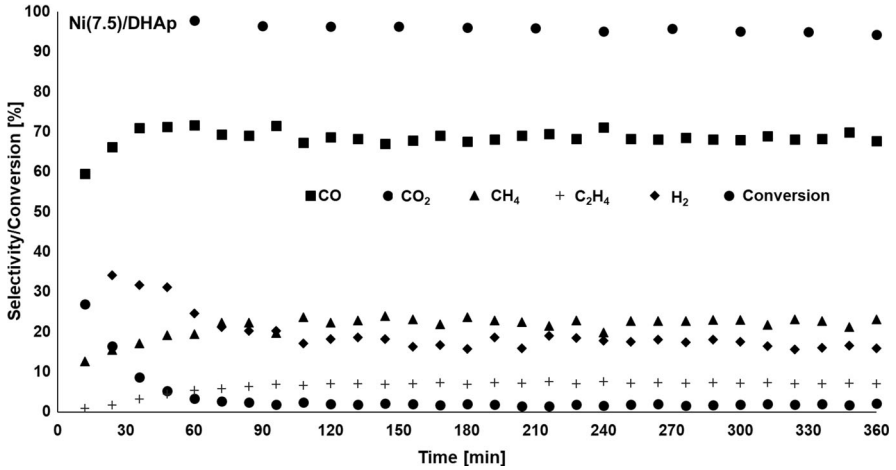

Fig. 10 Stability of Ni(7.5)/DHAp catalyst properties. Experimental conditions: 10 mg catalyst sample reduced in H_2 at 800 °C, S/C = 3, atmospheric pressure, isothermal test at 800 °C during 6 h on-stream

The catalysts selectivity to carbonaceous compounds (CO, CO_2, CH_4 and C_2H_4) has been evaluated. All tested catalysts provided a high selectivity to carbon monoxide (>70%). The received selectivity to carbon dioxide was very low, which means that the catalysts showed low activity in the water gas shift reaction (WGS). For the catalyst which was chosen as the most active in the glycerol reforming reaction (7.97 wt% of Ni), the selectivity to carbon dioxide were lower than 11% at 800 °C and rapidly drops with temperature decrease.

The low selectivity for hydrogen was accompanied by a rather high amount of hydrocarbons formed. Selectivities to methane were as high as 12–20% without significantly being affected by the steam reforming reaction temperature.

The differences between catalysts became apparent in the selectivity to ethylene, especially at the highest reaction temperatures ≥750 °C. Fig. 9 shows the changes in the selectivity to ethylene at temperatures of 750 and 800 °C with increasing nickel content. The lowest ethylene concentration was acquired by using the Ni(7.5)/DHAp catalyst at 800 °C. For comparison, 50 °C lower reaction temperature caused a raise of C_2H_4 selectivity from 3 up to 6%.

All catalysts show a high stability of its properties (activity and selectivity) during long-term tests. Fig. 10 presents results of 6-h glycerol reforming reaction over Ni(7.5)/DHAp catalyst at 800 °C. The catalyst presents both high stability of glycerol conversion (above 95%) and selectivity to gaseous products. There was only a slight change during the first hour of reaction run.

Conclusions

Nickel catalysts supported on nonstoichiometric hydroxyapatite showed both high activity and stability of its properties during glycerol steam reforming reaction. However, besides the mentioned benefits, they showed low selectivity towards hydrogen, and high to carbon monoxide. Despite these facts, this systems could be considered as catalysts for the preparation of synthesis gases with low H_2:CO_x ratio. Similar conclusions were made by Tran and Kannangara in their review [15]. They found that high-temperature processes, such as pyrolysis, steam reforming and oxidative steam reforming can provide synthesis gas with a H_2:CO_x ratio suitable for the synthesis of liquid fuels (methanol, dimethyl ether).

References

1. Biofuels OECD-FAO Agricultural Outlook 2015, OECD Publishing, Paris. http://www.oecd-ilibrary.org/agriculture-and-food/oecd-fao-agricultural-outlook-2015/biofuels_agr_outlook-2015-13-en;jsessionid=16npswsg2ycjz.x-oecd-live-02 Accessed 12 Feb 2017
2. Deutscher J, Sauerwald H (1986) J Bacteriol 166(3):829–836
3. Hettwer J, Oldenburg H, Flachsel E (2002) J Mol Catal B Enzym 19–20:215–222
4. Wang K, Hawley MC, DeAthos S (2003) J Ind Eng Chem Res 42(13):2913–2923
5. Zeng P (1996) Bioprocess Eng 14(4):169–175
6. Saint-Aman S, Perlot P, Goma G, Soucaille P (1994) Biotechnol Lett 16(8):831–836
7. Rokicki G, Rakoczy P, Parzuchowski P, Sobiecki M (2005) Green Chem 7:529–539
8. Clacens JM, Pouilloux Y, Barrault J (2002) J Stud Surf Sci Catal 143:687–695
9. Blanco M, Beneyto R, Castillo M, Porcel M (2004) Anal Chim Acta 521(2):143–148
10. Macierzanka A, Szeląg H (2004) Ind Eng Chem Res 43(24):7744–7753
11. Ott L, Bicker M, Vogel H (2006) Green Chem 8:214–220
12. Zhou CH, Zhao H, Tong DS, Wu LM, Yu WH (2013) Cat Rev Sci Eng 55(4):369–453
13. Gupta M, Kumar N (2012) Renew Sust En Rev 16(7):4551–4556
14. Stelmachowski M (2011) Ecol Chem Eng 18:9–30
15. Tran NH, Kannangara GSK (2013) Chem Soc Rev 42:9454–9479

16. Cortright RD, Davda RR, Dumesic JA (2002) Nature 418:964–967
17. Dauenhauer PJ, Salge JR, Schmidt LD (2006) J Catal 244(2):238–247
18. Byrd J, Pant KK, Gupta RB (2008) Fuel 87(13–14):2956–2960
19. Cichy M, Borowiecki T (2009) Przem Chem 9:995–1005
20. Lin Y-Ch (2013) Int J Hydrogen Energy 38(6):2678–2700
21. Bagnato G, Iuianelli A, Sanna A, Basile A (2017) Membranes 7:17–48
22. Silva JM, Soria MA, Madeira LM (2015) Renew Sustain Environ Rev 42:1187–1213
23. Silva JM, Soria MA, Madeira LM (2015) J Power Sources 273:423–430
24. Dou B, Song Y, Wang C, Chen H, Xu Y (2014) Renew Sustain Environ Rev 30:950–960
25. Hirai T, Ikenaga NO, Miyake T, Suzuki T (2005) Energy Fuel 19(4):1761–1762
26. Adhikari S, Fernando S, Haryanto A (2007) Catal Today 129:355–364
27. Zhang B, Tang X, Li Y, Xu Y, Shen W (2007) Int J Hydrogen Energy 32:2367–2373
28. Zhang B, Tang X, Li Y, Cai W, Xu Y, Shen W (2006) Catal Commun 7(6):367–372
29. Swami SM, Abraham MA (2006) Energy Fuel 20(6):2616–2622
30. Douette MD, Turn SQ, Wang W, Keffer VI (2007) Energy Fuel 21(6):3499–3504
31. Kunkes L, Simonetti DA, Dumesic JA, Pyrz WD, Murillo LE, Chen JG, Buttrey DJ (2008) J Catal 260:164–177
32. Simonetti DA, Kunkes EL, Dumesic JA (2007) J Catal 247(2):298–306
33. Iriondo A, Barrio VL, Cambra JF, Arias PL, Guemez MB, Navarro RM, Sanchez-Sanchez MC, Fierro JLG (2009) Catal Commun 10:1275–1278
34. Slinn M, Kendall K, Mallon C, Andrews J (2008) Bioresour Technol 99(13):5851–5858
35. Adhikari S, Fernando S, Haryanto A (2007) Energy Fuel 21(4):2306–2310
36. Soares RR, Simonetti DA, Dumesic JA (2006) Angew Chem Int Edit 45(24):3982–3985
37. Czernik S, French R, Feik C, Chornet E (2002) Ing Eng Chem Res 41(17):4209–4215
38. Adhikari S, Fernando SD, Haryanto A (2008) Renew Energy 33(5):1097–1100
39. Adhikari S, Fernando SD, Haryanto A (2009) Chem Eng Technol 32(4):541–547
40. Demash HD, Mohan R (2016) Int J Hydrogen Energy 41:22732–22742
41. Kim T, Park D (2017) J Nanosci Nanotechnol 17:2478–2481
42. Fu M, Xu Q, Qi W, Zhang Z, Zhang S, Yan Y (2016) Energy Source Part A 28:2128–2134
43. Lin KH, Lin WH, Hsiao CH, Chang HF, Chang ACC (2012) Int J Hydrogen Energy 37:13770–13776
44. Fleet ME, Liu X (2008) J Solid State Chem 181:2494–2500
45. Cruz FJAL, Canongia Lopes JN, Calado JCG (2005) J Phys Chem B 109:24473–24479
46. Kannan S, Rebelo A, Lemos AF, Barba A, Ferreira JMF (2007) J Eur Ceram Soc 27:2287–2294
47. Aellach B, Ezzamarty A, Leglise J, Lamonier C, Lamonier J-F (2010) Catal Lett 135:197–206
48. Yasukawa A, Gotoh K, Tanaka H, Kondori K (2012) Colloid Surf A 393:53–59
49. Hakim L, Yaakob Z, Ismail M, Wan Daud WR, Sari R (2013) Chem Pap 67:703–712
50. Joris SJ, Amberg CH (1971) J Phys Chem 75:3167–3171
51. Park JH, Lee D-W, Im S-W, Lee YH, Suh D-J, Jun K-W (2012) Fuel 94:433–439
52. Ashok J, Kumar SN, Subrahmannyam M (2007) Catal Lett 121:283–290
53. Yaakob Z, Hakim L, Kumar MNS, Ismail M, Wan Dau WR (2010) Am J Sci 1(2):122–126
54. Hakim L, Yaakob Z, Ismail M, Wan Daud WR (2010) Key Eng Mat 447–448:770–774
55. Hakim L, Yaakob Z, Ismail M, Wan Daud WR, Majlan EH (2011) Key Eng Mat 471–472:1046–1051
56. Nayak AK (2010) Int J ChemTech Res 2:903–907
57. Bobadilla LF, Penkova A, Romero-Sarria F, Centeno MA, Odriozola JA (2014) Int J Hydrogen Energy 39:5704–5712
58. Mustard DG, Bartholomew CH (1981) J Catal 67:186–206
59. Wu G, Zhang Ch, Li S, Han Z, Wang T, Ma X, Gong J (2013) ACS Sustain Chem Eng 1:1052–1062
60. Martinez LM, Araque M, Vargas JC, Roger AC (2013) Appl Catal B 132–133:499–510
61. Zanotto A, Saladino ML, Martino DC, Caponeti E (2012) Adv Nanoparticles 1:21–28
62. Scalera F, Gervaso F, Sanosh KP, Sannino A, Licciulli A (2012) Ceram Int 39:4839–4846
63. Jun JH, Lee T, Lim TH, Nam S, Hong S, Yoon KJ (2004) J Catal 221:178–190
64. Boukha Z, Kacimi M, Pereira MFR, Faria JL, Figueiredo JL, Ziyad M (2007) Appl Catal A 317:299–309
65. Miniach E, Śliwak A, Moyseowicz A, Gryglewicz G (2016) J Mater Sci 51:5367–5376